M. Islam, R. Martinez-Duarte "**The impact of using different renewable films in the synthesis and microstructure of carbonaceous materials applicable in origami-inspired manufacturing**" *Materialia*, 11, 100734 (2020).

The impact of using different renewable films in the synthesis and microstructure of carbonaceous materials applicable in origami-inspired manufacturing

Monsur Islam[†,‡] *and Rodrigo Martinez-Duarte*[†,*]

[†]Multiscale Manufacturing Laboratory, Mechanical Engineering Department, Clemson University, Clemson, SC 29634, USA

[‡] Institute for Microstructure Technology, Karlsruhe Institute of Technology, Hermann-von-Helmholtz-Platz 1, 76344 Eggenstein-Leopoldshafen, Germany

*Corresponding author: Email: rodrigm@clemson.edu (Rodrigo Martinez-Duarte)

ABSTRACT

Cellulose and starch are abundant biopolymers in nature and readily available in film or paper shape factor. Here, we present a comparative study of pure-cellulose chromatography paper, bacterial cellulose films, and starch in the form of rice paper as candidates for renewable base materials in the origami-inspired manufacturing of architected cellular structures made of carbon. Here, we elucidate the impact of the choice of biopolymer on the synthesis and microstructure of carbon and carbide materials obtained after heat treatment at temperatures 900-1300 °C. Depending on the precursor, either an entanglement of fibers or a stochastic foam-like microstructure was obtained. Bacterial cellulose showed significant promise to be a precursor material for a carbonaceous origami structure due to its nanofibril microstructure. All three biopolymers exhibited feasibility to be folded into complex origami structures. These results are of significant value towards replacing petroleum-based precursors with more sustainable ones in the manufacturing of lightweight carbonaceous parts.

Keywords: Biopolymers, Carbonaceous material, Origami, Porous, Architectured, Multiscale.

1. INTRODUCTION

Lightweight carbonaceous materials and structures are of interest in different applications due to their excellent chemical inertness, high thermal stability, low thermal expansion coefficient, low friction coefficient, electrical conductivity and mechanical strength.[1,2] Such properties have led to the disclosure of different techniques to fabricate porous carbonaceous structures that exhibit very low densities and high specific strength. Few examples include carbon nanotubes foams, graphene elastomers, carbon foams and carbon nanolattices.[3–6] However, these techniques mostly derive such carbonaceous materials from non-renewable precursors such as methane, coal tar, and pitch. Towards a renewable method to fabricate complex and cellular carbonaceous structures, we recently reported the use of origami techniques to fabricate very low-density cellular structures using cellulosic paper of plant origin as carbon precursor. We shaped the paper into complex structures using origami-based folding and then carbonized them at 900°C in an inert atmosphere, which resulted into 3D carbon origami structures.[7] These carbonaceous structures exhibited similar or better scaling and load carrying behavior than carbon nanotube foam and graphene elastomers.[8] Beyond carbon, we also functionalized the cellulose precursor with tungsten salt and folded it in to origami structures, followed by heat treatment at 1300°C in vacuum. This resulted in formation of 3D origami structures of tungsten carbide (WC).[9] We focused on the synthesis of tungsten carbide (WC) given its high elastic modulus when compared to that of carbon (600-700 GPa vs.10-40 GPa).[3,10] These origami structures can be potentially used as multi-functional materials owning to the structural properties of the origami architectures and the material and microstructural properties of the carbonaceous materials. For example, the WC origami structures exhibit good electrical conductance even under compressive load.[8,9] These results are promising for use of these carbonaceous origami structures as structural electrode materials in energy devices. In terms of manufacturing, an origami-enabled process can benefit from existent industrial infrastructure. For example, a roll of paper of various origins and dimensions can be fed to a continuous operation akin to newspaper printing. The paper can be creased using embossing, functionalized with different inks by roll printing or wall spraying, and folded using reprogrammable robots [11–13] or in a manner similar to the manufacturing of paper bags, filters,[14] or packaging containers.[15] These structures can then be heat treated in a rolling furnace, similar to the process used to fabricate tiles and various ceramic parts.[16]

Based on this promise, we speculated that other biopolymers could lead to the fabrication of paper origami, which can then be carbonized. In principle, any flexible sheet of carbon precursors can be folded into origami shapes. In this work, we chose three carbon precursors: paper made of plant cellulose, bacterial cellulose sheet and rice paper made from starch. These precursors were chosen based on their renewability, wide commercial availability and ability to be folded in to 3D complex origami shapes. Of special interest was the connection between the choice of biopolymer and the microstructure of the carbon material. The work presented here significantly expands our previous work by elucidating the effect of the choice between plant cellulose, bacterial cellulose and starch on the synthesis and microstructure of carbonaceous parts. Cellulose is the most abundant biopolymer in nature, with an approximate global production of 5×10^{11} metric tons.[17] Depending on the source, cellulose with different degrees of purity, crystallinity and dimensions can be obtained.[18–20] Although wood pulp remains the most important source for cellulose, cellulose is also produced by different algae and microbial strains such as *K. xylinus*. In particular, Bacterial Cellulose (BC) can be grown in a bioreactor and is known to feature a higher degree of purity and crystallinity than that extracted from plants.[21] Starch is also abundant. In 2000, the annual production of starch was estimated to be 48.5 million tons.[22] Due to the established industry around them, it is relatively easy to obtain large sheets of these renewable polymers; which makes them ideal candidates as the precursor to carbon in origami-inspired manufacturing.

The carbonization of plant cellulose, bacterial cellulose and starch has been investigated by other authors.[23–30] In our recent publication reporting the fabrication of carbon origami shapes from plant cellulose fibers, we discussed the effect of the carbon microstructures on the structural properties of the origami shapes.[7] However, choosing different biopolymers as the carbon precursor will lead to different microstructural properties. Furthermore, the material and microstructural properties of the carbon may have a major impact on the synthesis of the carbide materials, which is also a major topic of investigation in the field of carbide synthesis.[31,32] Hence, in this paper, we study the choice of these biopolymers on the synthesis of the metal carbide and on their folding feasibility towards fabricating carbonaceous origami shapes. Of note, the use of bacterial cellulose and starch is unexplored for the synthesis of metal carbides. The use of these biopolymers as carbon precursors in WC synthesis will expand the sustainable biopolymeric approach of carbide synthesis.

In this paper, we first compare the carbonization processes and carbon microstructures of chromatography paper to that of carbon obtained from films of bacterial cellulose and rice paper. We then present the effect of the choice of biopolymer on the synthesis and microstructure of WC, obtained by heat treating the paper functionalized with an aqueous solution of ammonium metatungstate (AMT). Lastly, we discuss the expected effects of the choice of carbon precursor on future carbon and WC origami structures and detail the practical challenges about using these precursors for fabrication of origami shapes.

2. EXPERIMENTAL SECTION

2.1. Materials.

Three renewable precursors were used in this work: chromatography (CG) paper, bacterial cellulose (BC) films, and rice paper. These will be referred to as biopolymer films throughout this paper. Pure cellulose chromatography paper with thickness of 0.19 mm was purchased from Fisher Scientific (Fisherbrand Chromatography Paper, Cat. No. 05-714-1). The BC pellicle was prepared following the synthesis procedure reported previously.[33,34] Briefly, *Komagataeibacter xylinus* (Formerly *Glucanoacetobater xylinus*) strain ATCC 700178 was cultured in Hestrin and Schramm (HS) media in 60 mm-diameter petri dishes for 14 days to attain a pellicle thickness of around 5 mm. The BC pellicle was washed in 0.1M NaOH solution for 12 hours to eliminate bacteria, followed by rinsing in distilled water until a neutral pH was achieved. Critical point drying (Quorum Technologies, United Kingdom) was performed in the case of BC pellicle so that the 3D interconnected nanofibril structure of BC is retained during the carbonization.[35] Rice paper was purchased as Banh Trang from Amazon.com (Three Ladies Brand). CG and rice paper were used as received.

Water-soluble ammonium meta-tungstate (AMT) was used as the tungstate precursor (Sigma Aldrich Cat. No. 463922). The use of an aqueous solution of AMT to infiltrate a carbon precursor for the synthesis of WC was previously reported.[36,37]

2.2. AMT infiltration.

20% (wt.%) AMT solution was prepared by adding 20g AMT in 100 ml of ultra-pure water and stirring on a magnetic stirrer (Thermolyne Nuova, United States) for 15 minutes. All the biopolymer films were immersed in the AMT solution for 15 minutes for infiltration, and immediately introduced into the tube furnace afterwards without any drying process in between. We picked a 20% AMT solution to infiltrate the carbon precursors based on our preliminary experiments with different concentration of AMT (see supplementary information).

2.3. Heat treatment.

All samples were carbonized in a tube furnace (TF1700, Across International, USA). Two heat treatment protocols were used. The first one was used for carbonization of the biopolymer films and featured a heating protocol detailed previously.[7] Briefly, (i) heating from room temperature to 300°C at a heating rate of 5°C/min; (ii) dwell at 300°C for 30 minutes to ensure complete removal of any oxygen in the heating tube; (iii) heating from 300°C to 900°C with a heating ramp of 5°C/min; (iv) dwell at 900°C for 75 minutes; and (v) cooling down to room temperature at a cooling rate of 5°C/min. The entire heat treatment process was carried out under nitrogen flow (10 standard cubic feet per hour).

The second protocol was used to heat treat the biopolymer films infiltrated with AMT and was similar to the one detailed above and reported in our previous publication.[9] Briefly, the final temperature was varied from 1100°C to 1300°C in the step (iii) to identify the lowest temperature to produce WC without any other crystalline phases; and a dwell time of 3 hours at the final temperature in step (iv). The entire heat-treatment process of the AMT-infiltrated samples was performed in a vacuum environment (vacuum pressure = -762 Torr). The vacuum environment was required because AMT is known to contain a highly stable form of WO_3 that requires high energy to break the stable W–O bond.[38]

2.4. Material Characterization.

Thermogravimetric analysis (TGA) was performed for the biopolymers in nitrogen environment up to 900°C with a heating rate of 5°C/min to determine the carbon yield of the biopolymers. The crystallinity and the composition of the heat-treated samples were characterized by X-ray diffraction (XRD) spectroscopy using Cu-Kα radiation (Rigaku Ultima IV, Japan). The XRD patterns were matched to different materials using the material database of International Centre for Diffraction Database (ICDD). Using the XRD pattern of the sample, the relative amount of the crystalline materials present in the sample was determined using Equation 1. We characterized the microstructure of the heat-treated samples using field emission scanning electron microscopy (FESEM, S4800, Hitachi, Japan). The grain size D in the heat-treated samples was estimated from the XRD patterns using the Scherrer equation (equation 2), which is only valid for grain sizes smaller than 100 nm,[39] using the wavelength of X-ray λ=1.5405 Å, the Bragg angle θ, the half width of the diffraction peak B and a constant k. The constant k is a dimensionless shape factor and the value of k ranges from 0.6366 to 1.5 depending on the shape of the crystallite.[39] In the abscense of the detailed shape of the crystallites, as is the case here, the use of $k = 0.9$ is preferred.[40]

$$Relative\ amount\ of\ X = \frac{Sum\ of\ the\ intensites\ of\ the\ peaks\ for\ X\ in\ XRD}{Sum\ of\ the\ intensities\ of\ all\ the\ peaks\ present\ in\ XRD} \times 100\% \tag{1}$$

$$D = \frac{k\alpha}{B\cos\theta} \tag{2}$$

3. RESULTS AND DISCUSSION

3.1. Analysis of renewable carbon precursors.

CG paper and BC are random networks of cellulose fibers (Figure 1a and c). The fibers in the CG paper used in this work are originally derived from wood pulp and are hollow, with an average fiber diameter of 17.48 ± 3.06 μm and an expected lumen diameter ranging from 8 μm to 12 μm as previously characterized by other authors.[41] During paper manufacturing, the lumen of fibers is likely to collapse by different amounts, yielding a highly variable microstructure in the paper.[42] The main constituent of CG paper, cellulose, is formed by the D-anhydroglucose ($C_6H_{10}O_5$) units linked by β-1,4-D-glucosidic bonds, which forms a chain-like structure. The presence of high number -OH functional groups on their surface make the cellulose fibers bond with water molecules with hydrogen bonds and makes the cellulose fibers highly hydrophilic.[43]

Bacterial cellulose is also an entanglement of cellulose fibers, Figure 1c, but as a result of the random 3D motion of bacteria in the culture. In contrast to CG paper, the cellulose fibers in BC are not hollow and feature an average fiber diameter of 80.09 ± 16.85 nm. The average spacing between the fibers ranges from 10 nm to 50 nm, much smaller than in the case of CG (0.7 to 30 μm). Due to such nanofibril structure, BC features a surface area 200 times higher than the plant cellulose fibers.[44] Furthermore, BC is known to be an extremely hydrophilic material, with water retention values up to 1000% [45] instead of 40-80% for cellulose of plant origin.[46] BC is also reported to exhibit higher purity, degree of polymerization (DP) and crystallinity than plant cellulose.[47] For example, BC features a DP ranging from 11000 and 17000, compared to 300 – 1700 for the plant cellulose in wood pulp.[47] Because of these properties, the folded structures derived from BC are expected to exhibit superior properties than the structures from CG paper.

The edible rice paper used here is marketed as gluten-free and prepared from rice flour, tapioca flour and additives such as protein, baking powder, oil, sugar and salt added in minor amounts.[48] Although the exact composition of the commercial rice paper used here was not available, we chose to study it based on its potential for origami-based manufacturing. The primary component of rice paper is starch,[49] which consists of two types of glucose polymers: (i) amylose and (ii) amylopectin.[50] Rice paper swells upon immersion in water, amylopectin has abundant -OH groups, yielding a soft, pliable film that enables its shaping in the wet state and maintains such shape after it dries. The microstructure of the rice paper resembles a dried paste-like morphology as shown in Figure 1e. This was expected as rice paper is prepared from the cooking of a thin spread batter of rice flour and tapioca flour followed by cooling and drying.[48]

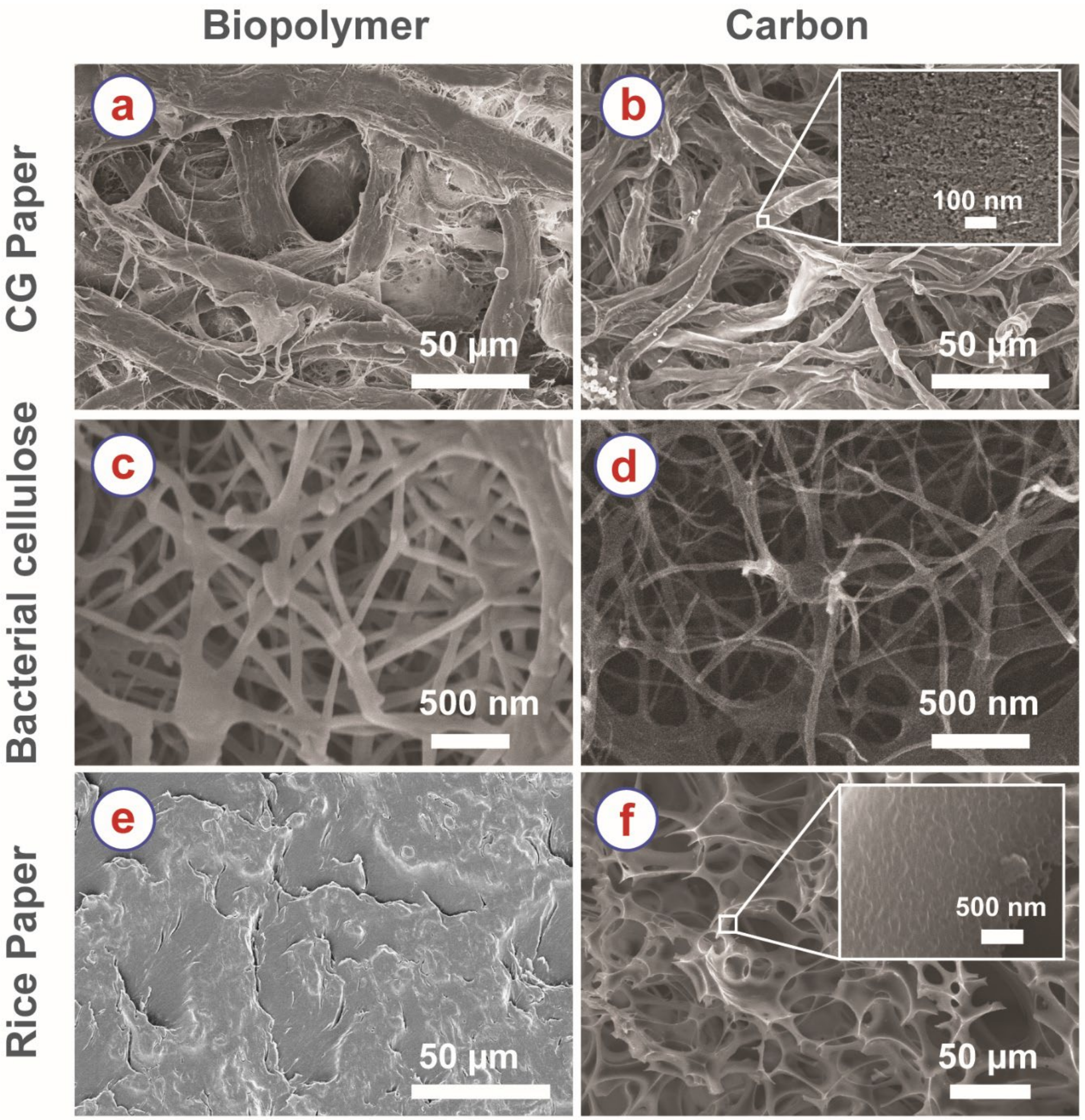

Figure 1. Microstructure of (a) CG paper, (c) BC and (e) rice paper. CG paper and BC feature a fibril network, whereas the microstructure of rice paper resembles a dried paste like structure. The biopolymers were carbonized at 900ºC in nitrogen environment. (b) Carbonized CG paper and (d) carbonized BC retains the fibril network of their respective precursor. Inset of figure (b) shows the mesoporous structure of each microfibers of

carbonized CG paper. (f) Upon carbonization rice paper yields a stochastic foam like structure. Inset shows the rough surface of each struct of this stochastic foam.

3.2. Composition and microstructure characterization of the pyrolyzed biopolymers.

The results from XRD and Raman spectroscopy are shown in Figure 2. In XRD, peaks centered around 2θ = 24° and 2θ = 43°, which are characteristic of the (002) and (100) planes of carbon of amorphous nature.[51] The difference in the sharpness of the peaks among the biopolymers suggested a variation in their crystallinity, which was confirmed by Raman spectroscopy. Two characteristic first order peaks can be observed in between 800 cm^{-1} and 2000 cm^{-1} in the Raman spectra of each carbon sample (Figure 2b). The peak at ~ 1340 cm^{-1} is referred as D-band, which represents the disordered carbon present in the sample. The other peak, which is at ~ 1580 cm^{-1} is G-band, representative of the crystalline planes of carbon present in the sample. Hence, the ratio of the intensities of D-band (I_D) and G-band (I_G) represents the degree of graphitization of the carbon sample.[52] For pure graphite, the ratio I_D/I_G approaches zero. The ratio for BC derived carbon is 1.43, whereas the ratio is 1.56 and 1.54 for rice paper and CG paper derived carbon respectively, clearly indicating that the carbon derived from BC is the most crystalline among the three carbon samples studied here.

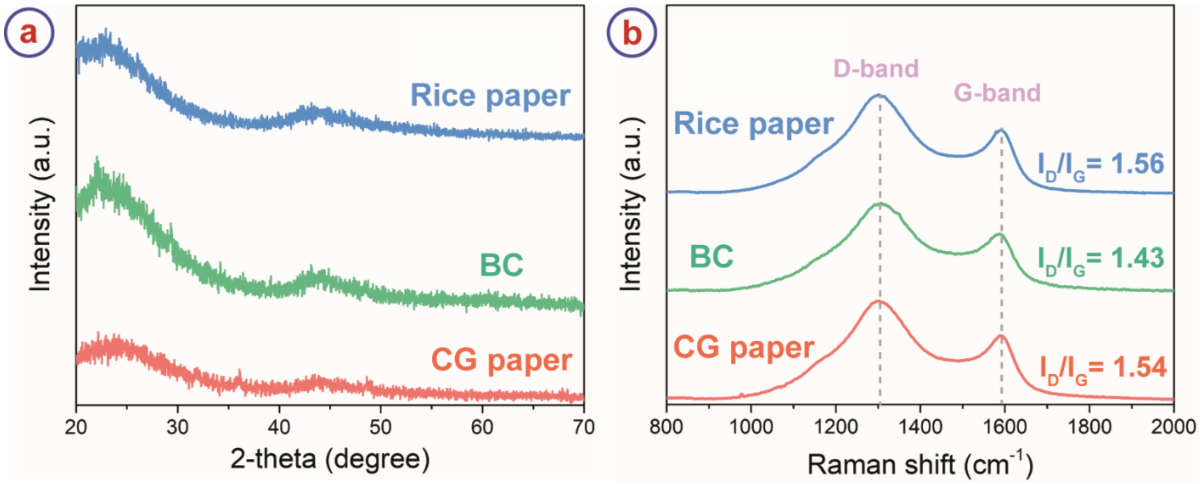

Figure 2. (a) XRD and (b) Raman spectra of the sample obtained after carbonization of CG paper, rice paper and BC at 900 °C in a nitrogen atmosphere.

The microstructure of the samples after carbonization shows different geometries and dimensions as illustrated in Figure 1b, d and f. The carbon sample derived from CG paper is a fibril network of randomly oriented carbon fibers with curls and kinks. The average diameter of the carbon fibers was 5.26 ± 2.53 µm, indicating a linear shrinkage of 69.89 ± 5.59% during carbonization. The structure exhibits macropores of varying dimensions ranging from 1.56 µm to 21.71 µm. Higher magnification SEM images showed mesoporous structure of the carbon fibers (inset of Figure 1b) with a pore diameter ranging from 3.15 nm to 44.78 nm. It should be noted here that these pore sizes were estimated based on the SEM images, which are basically the two-dimensional projections of the three-dimensional pores. Further studies such as nitrogen adsorption-desorption are required for precise measurement of the pore sizes. We could not perform it here because of the unavailability of the technique in the institute. The carbon fibers obtained from the CG paper were non-bonded and overlapped to each other. We suspect the thermal shrinkage due to the elimination of hydrogen and oxygen atoms caused the fibers to detach from each other, which would result in significantly weaker bonding among the fibers by van der Waal or coulombic forces. In addition, the thermal shrinkage resulted in the collapse of most of the lumen structures, yielding flattened fibers as shown in Figure 1b.

Carbonized BC is also a random network of fibrils which forms a three-dimensionally inter-connected network (Figure 1d). The carbon fibers from BC feature an average diameter of 21.33 ± 8.96 nm. Around 60% shrinkage of the fiber diameter occurred during the carbonization process. The interconnected network of the fibers resulted in many mesopores (pore size 2 nm – 50 nm) as estimated from the SEM images. The carbon nanofibers derived from BC are expected to contain micropores (pore size <2 nm) as well, as suggested by previous reports.[30,34] Like the CG paper, the bonding among the fibers due to van der Waal or coulombic forces is expected to be weaker than that of cellulose fibers.

In contrast to CG and BC paper, the carbonization of rice paper yields a stochastic foam of carbon featuring open cells, which is quite different from the microstructure of rice paper. The thickness of the carbonized rice sample also looked swollen when compared to the precursor rice paper. This is likely due to the use of baking powder as an additive in the rice paper preparation. We hypothesize the swallowing of the rice paper might have happened during the initial stage of heating, which caused a porous stochastic foam-like structure in the precursor itself. The carbonization might have occurred at the swollen state, which resulted in a stochastic foam like structure of carbonized structure. The distribution of the open cells is random, and the distant between the structs forming the open cells ranges from 12 to 250 µm as estimated from the SEM images. High magnification SEM of the struts of the stochastic foam shows that the struts feature a rough surface (Inset of Figure 1f).

The shape and dimensions of the material microstructure has an important role on its mechanical properties. In this case we have two different microstructures: an entanglement of fibers in CG and BC; and a stochastic foam in rice paper. Different models can be used to determine the mechanical properties of materials featuring such microstructures. For example, the elastic modulus of an entanglement of fibers can be characterized by the relation among the number of fiber segments in a unit sectional area, the distance between the connecting/support point of the fibers (length of suspended fiber segment) and the properties of a single fiber.[53,54] Upon loading, the stress is transferred through the structure until focusing on the fibers themselves, which emphasizes the importance of the fiber properties and the length of the suspended fibers. For example, different crystallinity and dimensions of the carbon fiber obtained from different precursor is expected to affect the modulus of the structure, while the density of fibers in the microstructure will determine the length of suspension. The diameter of carbon fibers derived from BC is significantly smaller than the diameter of carbon fibers from CG paper. The length of fiber suspension is also significantly smaller for BC-derived carbon because of its dense nanofibril microstructure. Hence, the mechanical properties of carbon paper from BC are expected to be superior than those from carbon derived from CG paper. As a result, the origami structures of BC derived carbon are expected to exhibit superior mechanical properties than that from CG derived carbon.

In contrast to a fiber entanglement, the microstructure of carbon derived from rice paper can be approximated as a stochastic foam (Figure 1f) characterized by the relation among the material properties of the constituent material, geometry of each strut and shape and size of an unit cell.[55,56] Due to bigger cell size, the carbon derived from rice paper is expected to yield lower mechanical properties when compared to CG paper and BC derived carbon. However, a bigger cell size will also result in low density for the rice paper derived carbon, which may result in higher specific strength and specific elastic modulus.

3.3. Carbon yield depending on the biopolymer.

We used TGA to estimate the carbon yield from each of the studied precursors. The carbon yield is important in the synthesis of carbonaceous materials to predict the final weight of pure carbon materials, their density and to assess the carbon present for reaction with other elements when developing carbides. In general, all the biopolymers exhibited similar TGA curves but with important differences in their carbon yield. The TGA curves for the biopolymers are presented in Figure 3. For CG paper, the carbon yield at 900ºC is only 4.3% of the initial weight, which is in agreement with that previously reported by other authors.[57] Of note, the thermal degradation of cellulose in CG started at 260°C, which corresponds to the reported temperature at which the β glyosidic bond of cellulose cleaves.[27] A drastic weight loss of 89.71% happened in the temperature range 260°C – 380°C and was attributed to the release of the volatile by-products of cellulose decomposition such as levoglucosan, hydroxyacetaldehyde, acetol, CO and CO_2 as previously reported.[58] Above 380°C, a gradual weight loss with a loss rate of 0.0097%/°C is observed, which is due to the escape of oxygen and hydrogen atoms as CO, CO_2 and C_xH_y.[23]

In contrast to CG, the carbon yield from BC is 20%. This difference was reported before[7,29,59]. We speculate that this difference occurs due to the difference in degree of polymerization (DP) between CG and BC. A higher DP represents a longer polymer chain. Sharma et al. suggested that, the hydrocarbon bonds break down to yield a highly disordered carbon short chains at a temperature ranging from 600ºC to 650ºC.[60] Upon an increase in temperature, the free carbon atoms of adjacent chains start forming carbon-carbon sp2 bonds among each other to make an ordered aromatic carbon chain. Two important parameters that influence this bonding process are the relative distance between the free carbon atoms and the rate of reaction between free carbon and hydrogen and oxygen to form volatile C_xH_y and CO_x groups. We speculate that the carbon chains in a precursor polymer with high DP remain closer to each other in the temperature range 600ºC – 650ºC. Thus, the carbon atoms may start forming sp^2 bonds with the adjacent atoms relatively easily, which also restricts the rate of production of volatile compounds. Further investigation is needed for verification of such speculation.

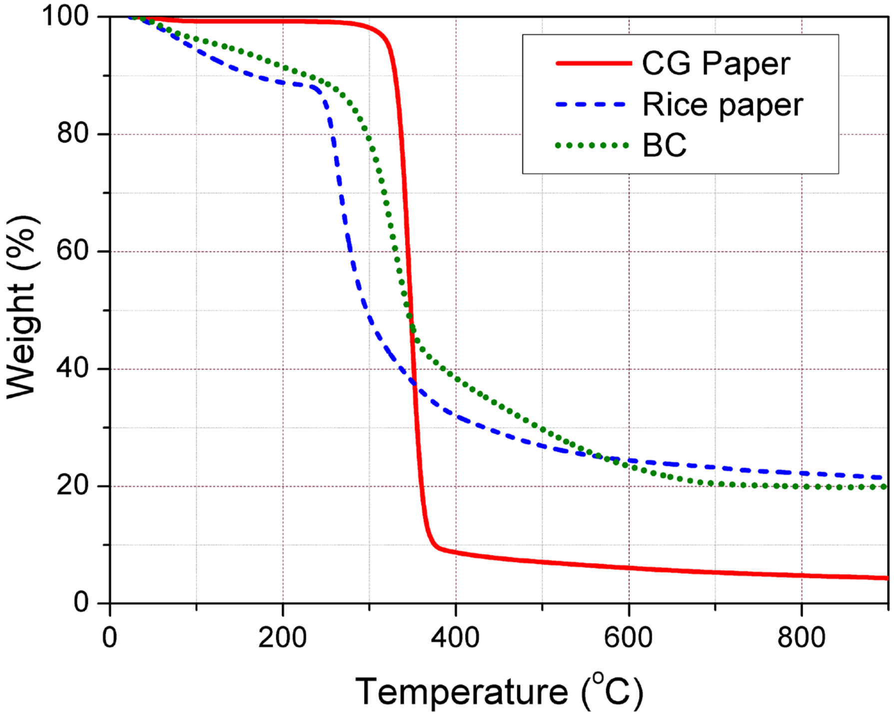

Figure 3. TGA of CG paper, BC and rice paper with a heating rate of 5°C/min in nitrogen environment.

The carbon yield of rice paper at 900°C was the highest of the three precursors at 21.4%. This value is also higher than the ~15% previously reported for starch.[28] We attribute this difference to the fact that the commercial rice paper used here has additives at unknown concentrations, including protein, oil, sugar and salt.[48] The mechanism of carbonization for starch is expected to be different from cellulose due to the presence of the amylose and amylopectin chains. For starch, the initiation point of the thermal decomposition, around 240ºC, depends on the ratio of amylose and amylopectin. For example, Liu et al reported that a corn starch with high amount of amylopectin, 77%, requires higher temperature, 275ºC, for thermal decomposition.[28] In the work presented here the initiation temperature of 240ºC might be attributed to the lower amylopectin content in rice starch (~30%) than corn starch.

3.4. The effect of carbon microstructure on the synthesis of tungsten carbide.

The XRD patterns of the samples obtained from all the three biopolymers infiltrated with 20% AMT and heat treated at different temperatures are presented in Figure 4. Three crystalline materials are clearly visible in the system: tungsten (W), tungsten carbide (WC) and tungsten hemicarbide (W_2C). The proportion of each of these materials in the samples depending on temperature is illustrated in Figure 4d. At 1100 °C, all the three biopolymers show a strong and dominant presence of metallic W, with WC being the other crystalline material in the sample. In the case of BC, small peaks for W_2C can already be observed in the XRD pattern. For all the three biopolymers, the amount of WC increases with increasing temperature, whereas the amount of metallic W decreases. This is obvious as the carburization of W depends on temperature. However, the reaction proceeded faster in the case of BC. The complete carburization of W particles happened at different temperatures depending on the choice of carbon precursor. For BC, the amount of metallic W becomes zero at a temperature of 1200°C, which signifies the complete carburization of W particles. In contrast to BC, the complete carburization of W particles occurred until 1300°C for both CG paper and rice paper to yield 73% and 91% WC respectively. At 1300°C, BC yielded around 93% WC. Hence, the use of BC yields a higher WC yield and seems to facilitate the reaction between W and C at lower temperatures when compared to CG and rice paper. This can be attributed to the crystallinity of the carbon obtained from the biopolymers as reported in a previous section (Figure 2). BC-derived carbon may require less energy in the carburization reaction due to the higher crystallinity of BC compared to the other precursors. This then results in lower carburization temperature for BC.

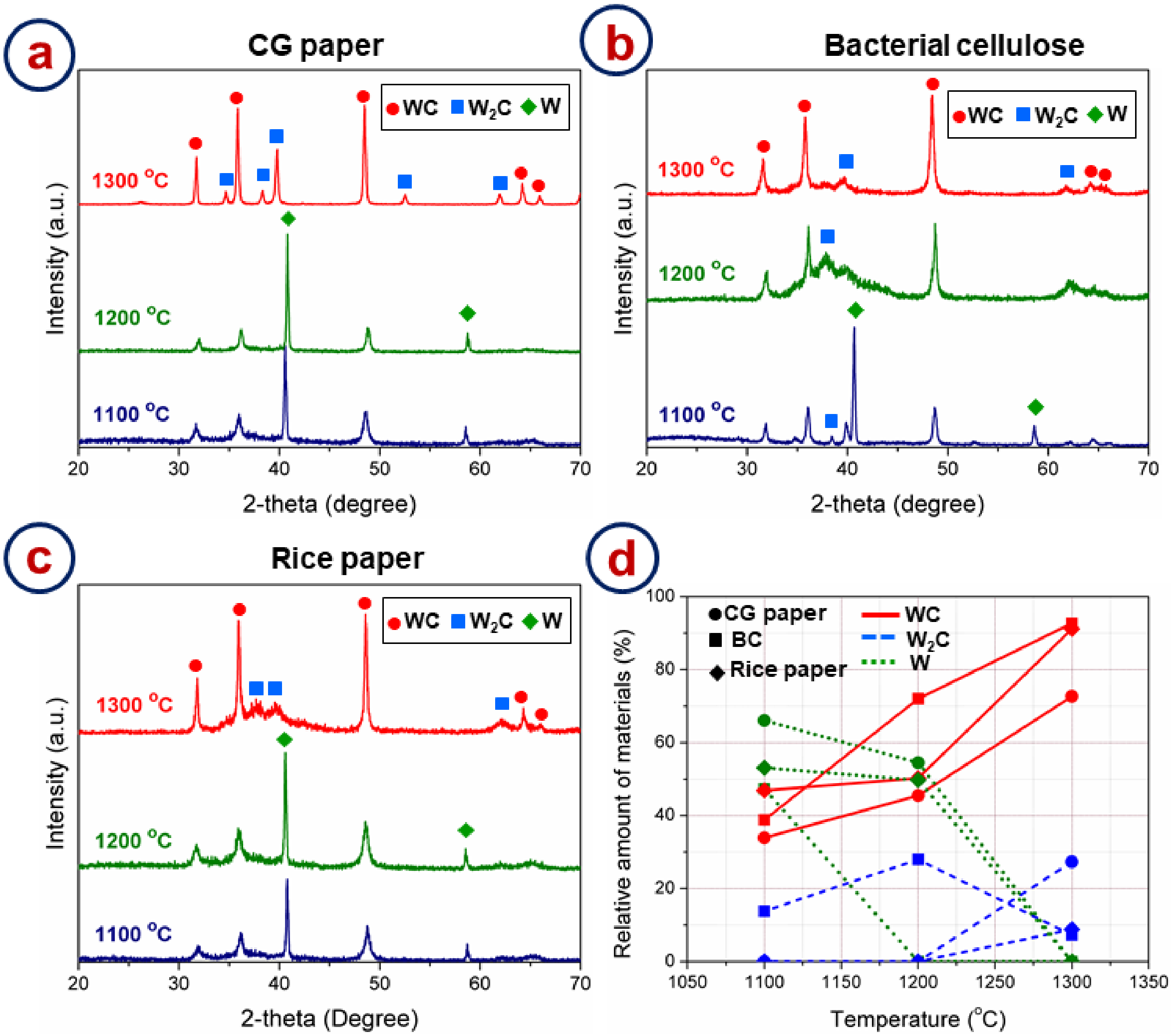

Figure 4. XRD patterns of (a) CG paper, (b) bacterial cellulose, and (c) rice paper infiltrated with 20% AMT solution and heat treated in a vacuum environment at a temperature ranging from 1100 °C to 1300 °C with a heating rate of 5 °C/min. (d) Relative amount of materials with temperature for all the three biopolymers.

W_2C remained present in all the samples at 1300°C. The highest W_2C percentage is 27% for CG paper while it is only 8 and 9% for BC and rice paper respectively. Our hypothesis is that these conditions can depend on the microstructure of the carbon material. The formation of W_2C is caused by the inefficient diffusion of the carbon atom through the metallic W particles. Ishii et al previously reported that this diffusion inefficiency mostly occurs for the metallic W particles sitting on the carbon surface.[61] They proposed the carburization starts on the surface of the tungsten particle, which is in contact with the carbon. The particles sitting on a carbon surface get transformed into WC only near the interfacial region due to direct vicinity of carbon. The diffusion through the WC region becomes challenging for the carbon residing under the WC region.[62] Hence, they result in incomplete carburization yielding formation of W_2C. We believe similar phenomenon occurred here in case of CG paper. CG fibers features an extended surface area in comparison to BC and rice paper and the dimensions of the fibers are an order of magnitude higher than the size of the tungsten particles. The average diameter of the cellulose fibers is 17.48 ± 3.06 µm and the lumen structures features a diameter ranging from 8 µm to 12 µm, leading to hollow carbon fibers of thickness of 5-9 µm. On the contrary, BC fibers are solid and feature a diameter of 80.09 ± 16.85 nm. The grain size of the W particles reported here was between 28 and 68 nm (see supplementary information). Hence, comparing the W particle size with the fiber dimensions of the CG paper, it is highly possible that a significant number of W particles might be nucleated on the carbon surfaces during the reduction step. These W particles sitting on the carbon surface might experience insufficient diffusion of carbon, which led to formation of higher amount of W_2C at a higher temperature. In the case of BC, the fiber diameter is comparable to the size of the expected W particles. This might facilitate the carburization process yielding formation of higher amount of WC. However, in case of rice paper, the expected nucleation of the tungsten particles might occur within the carbon matrix. This is because, starch is known to form a sol in presence of water through hydration reaction.[24] As a characteristic of sol material, the reactions occur in close proximity of the reactants,[32] which may promote the carbon diffusion into the tungsten particles. This resulted in formation of more WC for rice paper when compared to CG paper.

3.5. Microstructure of the WC obtained from the biopolymers.

Figure 5a and b show the morphology of the WC obtained from the CG paper and BC respectively. In both cases, the WC retained the fibril structure of its precursor, but the fiber dimensions increased in different degrees. The average fiber diameter of the WC fibers from CG paper was 10.34 ± 2.79 µm, which is larger than the diameter of the fibers obtained after carbonization of the untreated cellulose fibers at 900°C. The nucleation of the crystalline intermediates inside the carbon matrix during the reduction of AMT may hinder the thermal shrinkage of the fibers, which yield larger fiber diameter than the carbon fibers.

In the case of WC derived from BC, the average diameter of the fibers is 177.16 ± 17.11 nm, which is almost 2 times larger than the carbonized fibers from BC. We hypothesize that the hydrophilic nature of the BC is responsible for such increase in the diameter. As we mentioned earlier, BC is known to be an extremely hydrophilic material showing a water retention value up to 1000%.[45] Because of such high hydrophilic nature, BC fibers swell in presence of water. We suspect the nucleation of the crystalline intermediate particles started at such swollen state of the BC fibers. The W particles reduced from AMT featured a particle size ranging from 28 to 68 nm (Figure S2 in supplementary information), comparable to the diameter of the BC fibers, as estimated from the XRD plots using Scherrer equation. Hence, we expect that the carburization reaction between these components of comparable dimensions results in a fiber diameter larger than the diameter of the precursor material.

The rice paper lost its unique cellular structure and formed a porous structure of the agglomerated WC particles during the formation of WC. As starch forms a sol in presence of water through hydration reaction,[24] the rice paper loses its unique cellular structure in reaction with water. Hence, here the starting material for WC synthesis is a starch sol infiltrated with AMT solution. The carbide synthesized from an aqueous sol precursor is expected to feature a porous structure of agglomerated grains of carbides,[31] which agrees to the microstructure of our final product obtained from the heat treatment of AMT infiltrated rice paper. The average grain size of the WC synthesized from the rice paper is estimated to be 38.76 ± 6.27 nm.

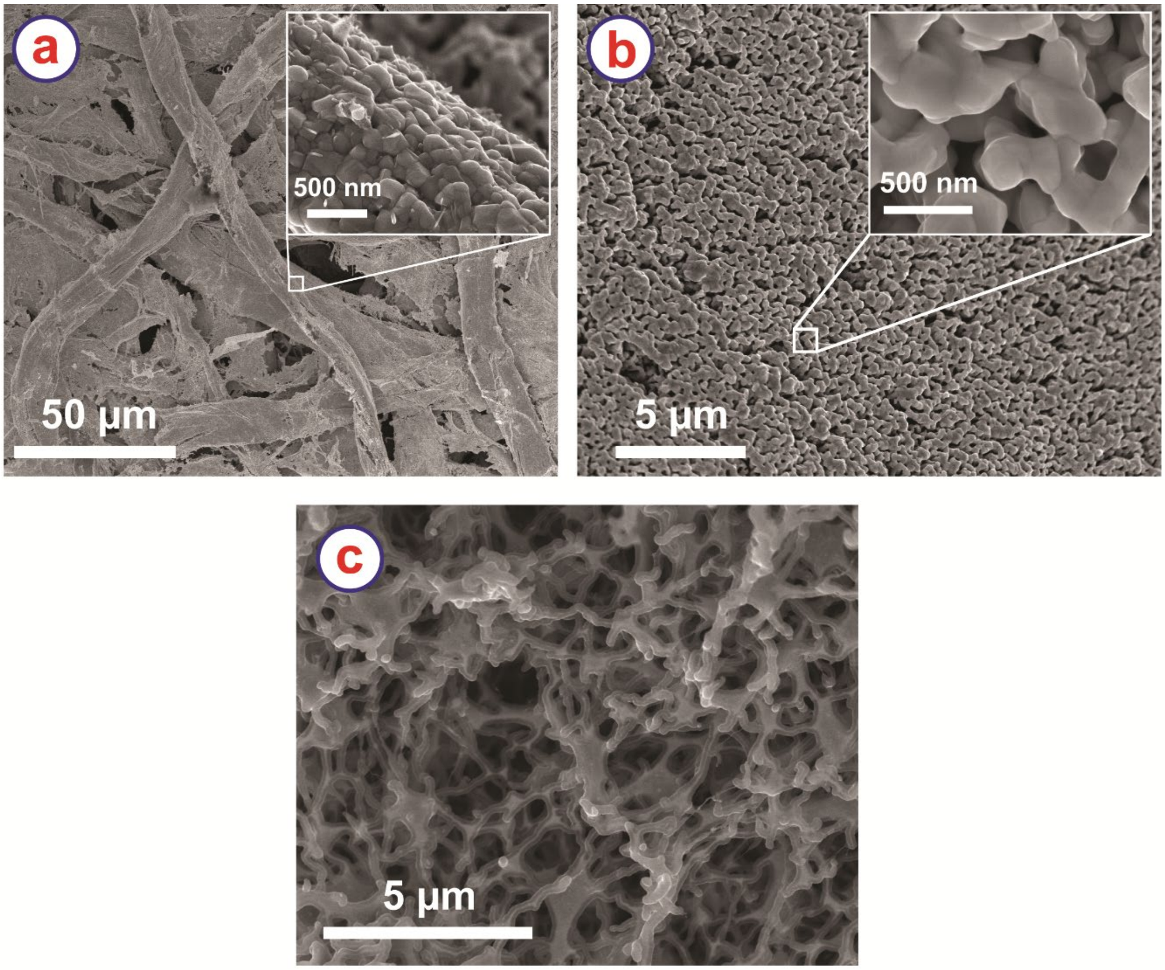

Figure 5. FESEM images of the WC obtained from (a) CG paper, (b) BC, and (c) rice paper infiltrated with 20% AMT and heat treated at 1300 °C in a vacuum environment. WC from both CG paper and BC retains the fibril structure of their bio-precursors. WC from rice paper loses the cellular structure and forms a porous agglomeration of particles.

3.6. Foldability Assessment.

The parameter which is most important to fabricate 3D complex origami shapes is foldability of the precursor papers. CG paper can be easily folded into 3D complex origami shapes (Figure 6a). The carbon and WC samples obtained from the folded CG papers are shown in the Figure 6b and 6c respectively. Both carbon and WC retained the shapes of the precursor CG paper, although a significant shrinkage occurred during the heat treatment.

Carbon and WC origami derived from CG paper are detailed in our previous publications.[7,9] In contrast to CG paper, foldability of the BC sheet and rice paper into origami shapes is less straightforward. In wet conditions, handling BC sheets or rice paper is difficult as it is prone to tear apart. On the contrary, BC sheets and rice papers are brittle at dry state. Our preliminary experiments with the dried BC sheet and rice paper resulted in cracks or fractures of the sheet during pre-creasing and folding. One possible solution to facilitate the folding is to apply oil on the precursor sheet, which provides the precursor sheets extra flexibility for folding. Example of an origami shape fabricated using an oiled BC sheet is shown in Figure 6d. However, the addition of oil in the system might have some significant effect on the synthesis process of WC, which needs to be thoroughly investigated. Another possible solution is to use external molds to shape the BC sheet or rice paper in wet conditions and let them dry inside the mold. Examples of such molded origami with rice paper are shown in Figure 6e. The carbon obtained from the folded rice paper did not retain the origami shape of the precursor (see Figure S3 in supplementary information), because the thickness of the carbon gets bigger than the rice paper as we mentioned earlier. The rice paper needs further chemical treatment to suppress the expansion behavior during carbonization, which can yield to formation of the carbonaceous origami structures from rice paper. The ongoing work focuses on finding a suitable method to fold the BC sheet and rice paper in their purest biopolymer form, which will lead to the fabrication of the carbonaceous origami structures from these biopolymers.

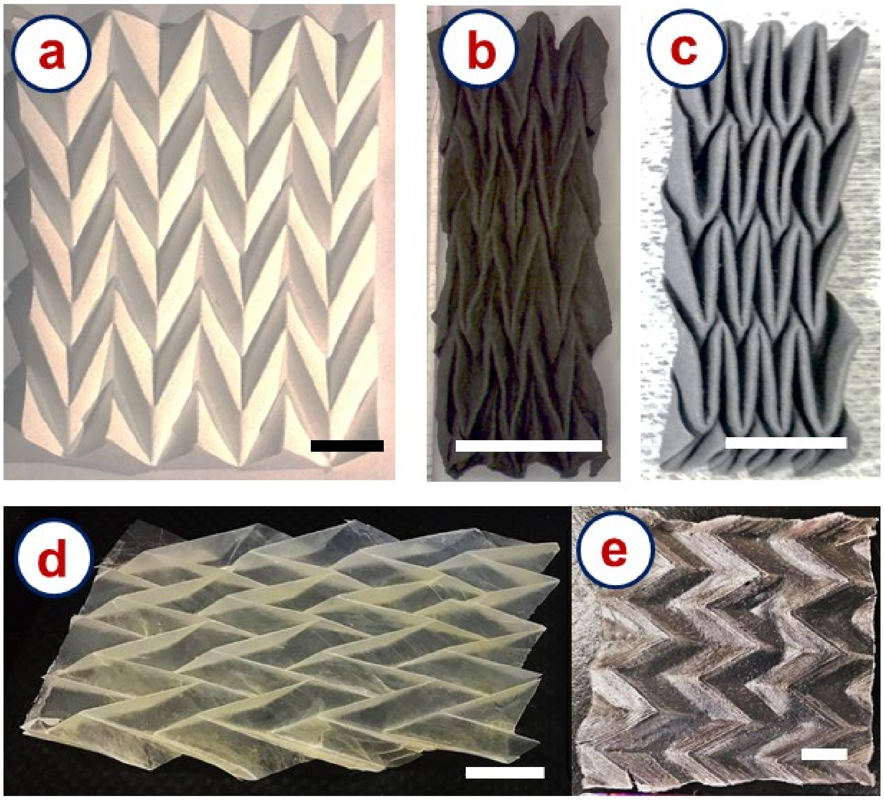

Figure 6. (a) Miura-ori shape of CG paper fabricated by automatic pre-creasing and manual folding. (b) Carbon and (c) WC origami shapes obtained from CG paper. Note that, both carbon and WC retained the shape of the precursor CG paper. (d) Miura-ori shape of bacterial cellulose sheet fabricated by applying oil on the BC sheet to increase its flexibility followed by pre-creasing and manual folding. (e) Miura-ori shape of rice paper fabricated by molding the wet rice paper in a mold and letting it dry inside the mold. All the scale bars are 1 cm.

4. CONCLUSION

In this work we studied the effect of three biopolymers, pure cellulose chromatography paper, bacterial cellulose films and rice paper, on the synthesis and microstructure of carbon and WC materials and discussed their use as potential carbon precursors for the fabrication of carbon and WC origami structures. The carbon and WC from CG paper and BC featured a fibril microstructure. The carbon obtained from rice paper featured a stochastic foam-like microstructure, whereas the WC from rice paper featured a porous structure of agglomerated

WC particles. Among the three biopolymers, BC showed the highest promise to be a precursor material for a carbonaceous origami structure due to its nanofibril microstructure and ability to produce higher crystalline material at a relatively low temperature. However, fabrication of carbonaceous origami structures from BC and rice paper involves extreme challenges, although the biopolymer sheets can be folded into origami shapes. Ongoing work is on using the BC paper and rice paper for fabrication of WC and carbon origami structures and compare the structural properties of the carbonaceous materials from these biopolymers.

ACKNOWLEDGEMENTS

Monsur Islam acknowledges support from Hitachi through a High Technologies Fellowship. The authors thank to several colleagues at Clemson University: Devin Keck from the Multiscale Manufacturing Laboratory for helping with preparation of bacterial cellulose pellicle; Dr. Taghi Darroudi and Dr. Laxmikant Saraf from the Electron Microscopy (EM) Laboratory for advice during image acquisition; and Dr. Kimberly Ivy from the Analytical Measurement Laboratory for facilitating TGA studies.

The authors declare no conflict of interest.

REFERENCES:

1. Fang, Z. Z., Wang, X., Ryu, T., Hwang, K. S. & Sohn, H. Y. Synthesis, sintering, and mechanical properties of nanocrystalline cemented tungsten carbide - A review. *Int. J. Refract. Met. Hard Mater.* **27**, 288–299 (2009).
2. Sakintuna, B. & Yürüm, Y. Templated porous carbons: A review article. *Ind. Eng. Chem. Res.* **44**, 2893–2902 (2005).
3. Szczurek, A. *et al.* Carbon periodic cellular architectures. *Carbon N. Y.* **88**, 70–85 (2015).
4. Chen, C., Kennel, E. B., Stiller, A. H., Stansberry, P. G. & Zondlo, J. W. Carbon foam derived from various precursors. *Carbon N. Y.* **44**, 1535–1543 (2006).
5. Qiu, L., Liu, J. Z., Chang, S. L. Y., Wu, Y. & Li, D. Biomimetic superelastic graphene-based cellular monoliths. *Nat. Commun.* **3**, 1–7 (2012).

6. Worsley, M. A., Kucheyev, S. O., Satcher, J. H., Hamza, A. V. & Baumann, T. F. Mechanically robust and electrically conductive carbon nanotube foams. *Appl. Phys. Lett.* **94**, 1–4 (2009).

7. Islam, M., Flach, J. & Martinez-Duarte, R. Carbon Origami: A Method to Fabricate Lightweight Carbon Cellular Materials. *Carbon N. Y.* **133**, 140–149 (2018).

8. Islam, M. *Advanced Manufacturing of Lightweight Porous Carbide Shapes Using Renewable Resources*. *ProQuest Dissertations and Theses* (2018).

9. Islam, M., Keck, D. & Martinez-Duarte, R. Architected Tungsten Carbide Electrodes Using Origami Techniques. *Adv. Eng. Mater.* 1–14 (2019). doi:10.1002/adem.201900290

10. Carbide, G. *The Designer ' s Guide to Tungsten Carbide*. (2007).

11. Namiki, A. & Yokosawa, S. Robotic origami folding with dynamic motion primitives. *IEEE Int. Conf. Intell. Robot. Syst.* **2015-Decem**, 5623–5628 (2015).

12. Tanaka, K., Kamotani, Y. & Yokokohji, Y. Origami folding by a robotic hand. *IEEE Int. Conf. Intell. Robot. Syst.* 2540–2547 (2007). doi:10.1109/IROS.2007.4399358

13. Liu, H. & Dai, J. An approach to carton-folding trajectory planning using dual robotic fingers. *Rob. Auton. Syst.* **42**, 47–63 (2003).

14. Zhao, C., Peng, Q. & Gu, P. Development of a paper-bag-folding machine using open architecture for adaptability. *Proc. Inst. Mech. Eng. Part B J. Eng. Manuf.* **229**, 0954405414559281 (2015).

15. Jones, H. G. Tetra Pak -- A model for Successful Innovation. *Long Range Plann.* **15**, 31–37 (1982).

16. Celik, H., Samanli, S. & Öney, Ö. The use of tincal calcination plant waste as an additive in ceramic wall tile production. *J. Ceram. Process. Res.* **15**, 508–513 (2014).

17. Qiu, X. & Hu, S. 'Smart' materials based on cellulose: A review of the preparations, properties, and applications. *Materials (Basel).* **6**, 738–781 (2013).

18. Endes, C. *et al.* A critical review of the current knowledge regarding the biological impact of nanocellulose. *J. Nanobiotechnology* **14**, 1–14 (2016).

19. Islam, M. T., Alam, M. M., Patrucco, A., Montarsolo, A. & Zoccola, M. Preparation of Nanocellulose: A Review. *AATCC J. Res.* **1**, 17–23 (2014).

20. Kim, J. H. *et al.* Review of nanocellulose for sustainable future materials. *Int. J. Precis. Eng. Manuf. - Green Technol.* **2**, 197–213 (2015).

21. Moon, R. J., Martini, A., Nairn, J., Simonsen, J. & Youngblood, J. Cellulose nanomaterials review: structure, properties and nanocomposites. *Chem. Soc. Rev.* **40**, 3941–3994 (2011).

22. Corre, D. Le & Dufresne, A. Starch Nanoparticles : A Review Starch Nanoparticles : A Review. *Biomacromolecules* **11**, 1139–1153 (2010).

23. Li, S., Lyons-Hart, J., Banyasz, J. & Shafer, K. Real-time evolved gas analysis by FTIR method: An experimental study of cellulose pyrolysis. *Fuel* **80**, 1809–1817 (2001).

24. Chang, X., Chen, D. & Jiao, X. Starch-derived carbon aerogels with high-performance for sorption of cationic dyes. *Polymer (Guildf).* **51**, 3801–3807 (2010).

25. Katō, K. & Komorita, H. Pyrolysis of cellulose Part IV. Effect of crystallinity of cellulose on the formation of volatile compounds. *Agric. Biol. Chem.* **32**, 21–26 (1968).

26. Musa, M. *et al.* Characterization and thermomechanical properties of thermoplastic potato starch. *J. Eng. Technol.* **2**, 9–16 (2013).

27. Shen, D. K. & Gu, S. The mechanism for thermal decomposition of cellulose and its main products. *Bioresour. Technol.* **100**, 6496–6504 (2009).

28. Liu, X. *et al.* Kinetics and mechanism of thermal decomposition of cornstarches with different amylose/amylopectin ratios. *Starch/Staerke* **62**, 139–146 (2010).

29. Štefelová, J. *et al.* Drying and Pyrolysis of Cellulose Nanofibers from Wood, Bacteria, and Algae for Char Application in Oil Absorption and Dye Adsorption. *ACS Sustain. Chem. Eng.* **5**, 2679–2692 (2017).

30. Wang, W., Sun, Y., Liu, B., Wang, S. & Cao, M. Porous carbon nanofiber webs derived from bacterial cellulose as an anode for high performance lithium ion batteries. *Carbon N. Y.* **91**, 56–65 (2015).

31. Islam, M. & Martinez-Duarte, R. A sustainable approach for tungsten carbide synthesis using renewable biopolymers. *Ceram. Int.* **43**, 10546–10553 (2017).

32. Schnepp, Z., Wimbush, S. C., Antonietti, M. & Giordano, C. Synthesis of highly magnetic iron carbide nanoparticles via a biopolymer route. *Chem. Mater.* **22**, 5340–5344 (2010).

33. Iguchi, M., Yamanaka, S. & Budhiono, a. Bacterial cellulose - a masterpiece of nature's arts. *J. Mater. Sci.* **35**, 261–270 (2000).

34. Chen, L. F., Huang, Z. H., Liang, H. W., Gao, H. L. & Yu, S. H. Three-dimensional heteroatom-doped carbon nanofiber networks derived from bacterial cellulose for supercapacitors. *Adv. Funct. Mater.* **24**, 5104–5111 (2014).

35. Tang, W., Jia, S., Jia, Y. & Yang, H. The influence of fermentation conditions and post-treatment methods on porosity of bacterial cellulose membrane. *World J. Microbiol. Biotechnol.* **26**, 125–131 (2010).

36. Ganesan, R. & Lee, J. S. Tungsten carbide microspheres as a noble-metal-economic

electrocatalyst for methanol oxidation. *Angew. Chemie - Int. Ed.* **44**, 6557–6560 (2005).

37. Ma, C., Sheng, J., Brandon, N., Zhang, C. & Li, G. Preparation of tungsten carbide-supported nano Platinum catalyst and its electrocatalytic activity for hydrogen evolution. *Int. J. Hydrogen Energy* **32**, 2824–2829 (2007).

38. Joo, J. B., Kim, J. S., Kim, P. & Yi, J. Simple preparation of tungsten carbide supported on carbon for use as a catalyst support in a methanol electro-oxidation. *Mater. Lett.* **62**, 3497–3499 (2008).

39. Langford, J. I. & Wilson, A. J. C. Scherrer after sixty years: A survey and some new results in the determination of crystallite size. *J. Appl. Crystallogr.* **11**, 102–113 (1978).

40. Holzwarth, U. & Gibson, N. The Scherrer equation versus the 'Debye-Scherrer equation'. *Nat. Nanotechnol.* **6**, 534–534 (2011).

41. Ververis, C., Georghiou, K., Christodoulakis, N., Santas, P. & Santas, R. Fiber dimensions, lignin and cellulose content of various plant materials and their suitability for paper production. *Ind. Crops Prod.* **19**, 245–254 (2004).

42. Marulier, C., Dumont, P. J. J., Org??as, L., Rolland du Roscoat, S. & Caillerie, D. 3D analysis of paper microstructures at the scale of fibres and bonds. *Cellulose* **22**, 1517–1539 (2015).

43. Medronho, B. & Lindman, B. Brief overview on cellulose dissolution/regeneration interactions and mechanisms. *Adv. Colloid Interface Sci.* **222**, 502–508 (2015).

44. Henriksson, M., Berglund, L. A., Isaksson, P., Lindstro, T. & Nishino, T. Cellulose Nanopaper Structures of High Toughness. *Biomacromolecules* **9**, 1579–1585 (2008).

45. Klemm, D., Schumann, D., Udhardt, U. & Marsch, S. Bacterial synthesized cellulose—artificial blood vessels for microsurgery. *Prog. Polym. Sci.* **26**, 1561–1603 (2001).

46. Blazek, J. & Copeland, L. Pasting and swelling properties of wheat flour and starch in relation to amylose content. *Carbohydr. Polym.* **71**, 380–387 (2008).

47. Klemm, D., Heublein, B., Fink, H. P. & Bohn, A. Cellulose: Fascinating biopolymer and sustainable raw material. *Angew. Chemie - Int. Ed.* **44**, 3358–3393 (2005).

48. M. H. Abdel-Haleem, A. Production of Gluten-Free Rolled Paper from Broken Rice by Using Different Hydrothermal Treatments. *Int. J. Nutr. Food Sci.* **5**, 255 (2016).

49. Cameron, S. J. & Hosseinian, F. Potential of flaxseed in the development of omega-3 rice paper with antioxidant activity. *LWT - Food Sci. Technol.* **53**, 170–175 (2013).

50. Van Der Maarel, M. J. E. C., Van Der Veen, B., Uitdehaag, J. C. M., Leemhuis, H. & Dijkhuizen, L. Properties and applications of starch-converting enzymes of the α-

amylase family. *Journal of Biotechnology* **94**, 137–155 (2002).

51. Palmre, V. *et al.* Electroactive polymer actuators with carbon aerogel electrodes. *J. Mater. Chem.* **21**, 2577 (2011).

52. Li, J. G., Tsai, C. Y. & Kuo, S. W. Fabrication and characterization of inorganic silver and palladium nanostructures within hexagonal cylindrical channels of mesoporous carbon. *Polymers (Basel).* **6**, 1794–1809 (2014).

53. Markaki, A. E. & Clyne, T. W. Magneto-mechanical actuation of bonded ferromagnetic fibre arrays. *Acta Mater.* **53**, 877–889 (2005).

54. Picu, R. C. Mechanics of random fiber networks - A review. *Soft Matter* **7**, 6768–6785 (2011).

55. Roberts, A. P. & Garboczi, E. J. Elastic properties of model random three-dimensional open- cell solid. *J. Mech. Phys. Solids* **50**, 33–55 (2002).

56. Li, K., Gao, X. L. & Subhash, G. Effects of cell shape and strut cross-sectional area variations on the elastic properties of three-dimensional open-cell foams. *J. Mech. Phys. Solids* **54**, 783–806 (2006).

57. Yeng, L. C., Wahit, M. U. & Othman, N. Thermal and flexural properties of regenerated cellulose (RC)/ poly(3-hydroxybutyrate) (PHB) biocomposites. *J. Teknol.* **75**, 107–112 (2015).

58. Shen, D., Xiao, R., Gu, S. & Zhang, H. The Overview of Thermal Decomposition of Cellulose in Lignocellulosic Biomass. in *Cellulose - Biomass Conversion* 193–226 (2013). doi:10.5772/51883

59. De Souza, C. F. *et al.* Property evaluations of dry-cast reconstituted bacterial cellulose/tamarind xyloglucan biocomposites. *Carbohydr. Polym.* **93**, 144–153 (2013).

60. Sharma, S. *et al.* Micro and nano patternable magnetic carbon. *J. Appl. Phys.* **120**, (2016).

61. Ishii, T., Yamada, K., Osuga, N., Imashiro, Y. & Ozaki, J. I. Single-Step Synthesis of W2C Nanoparticle-Dispersed Carbon Electrocatalysts for Hydrogen Evolution Reactions Utilizing Phosphate Groups on Carbon Edge Sites. *ACS Omega* **1**, 689–695 (2016).

62. Hoier, P. Effect of Carbon Sources and Carbonaceous Atmospheres on the Effective Synthesis of Nanostructured Tungsten Carbide Powders. (Chalmers University of Technology, 2014).

SUPPLEMENTARY INFORMATION:

To determine the amount of ammonium metatungstate (AMT) needed to synthesize tungsten carbide (WC) from the biopolymers, we first infiltrated the biopolymers with different concentration of AMT ranging from 10% to 50%. The infiltrated biopolymers were heat treated at 1300 °C for 3 hours in vacuum with a heating rate of 5 °C/min. The XRD patterns of the heat-treated samples are shown in Figure S1. For all the biopolymers, an AMT concentration more than 50% resulted in metallic tungsten (W) in the matrix. For 10% and 20% AMT, no peaks for metallic W can be seen. However, significant amount of amorphous carbon was present in the samples as suggested by the bulged portion of the XRD pattern in the range from 2θ = 20° to 2θ = 30°. In the samples for both 10% and 20% AMT, the main crystalline phase materials were WC and tungsten hemicarbide (W_2C). It should be noted that, the intensities for the peaks of WC were higher for the samples obtained from 20% AMT compared to that from 10% AMT. This suggests higher formation of WC occurred in case of 20% AMT, which further suggests presence of lower amount of carbon in the matrix. Hence, comparing the different concentrations of AMT, 20% AMT seems to be the concentration which produces highest amount of WC in our system. We continued our further experiments with 20% AMT.

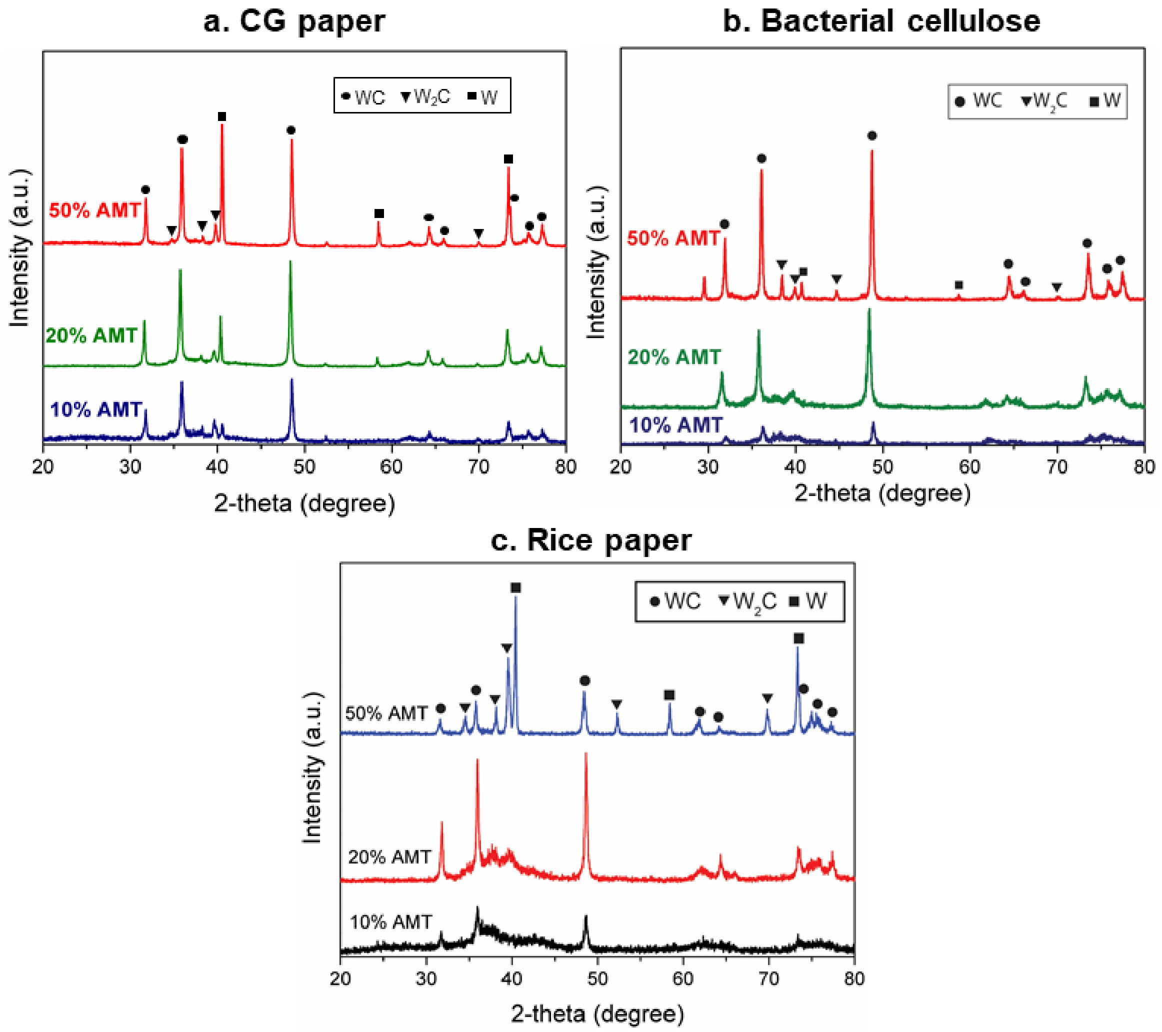

Figure S1: XRD of the heat-treated samples obtained from (a) Chromatography (CG) paper, (b) bacterial cellulose, and (c) rice paper infiltrated with different amount of ammonium metatungstate (AMT) and heat treated at 1300 °C for 3 hours in vacuum environment with a heating rate of 5 °C/min.

The average grain size of the W particle was estimated from the XRD plots using Scherrer equation. The samples were obtained by heat treating the biopolymers infiltrated with 20% AMT. A constant heating rate of 5 °C/min and vacuum environment were implemented during the heat treatment. The grain size of the tungsten particle for each biopolymer at different temperature was presented in Figure S2. At 1300 °C, no peaks for W were observed. Hence, grain size for W is reported here up to 1200 °C.

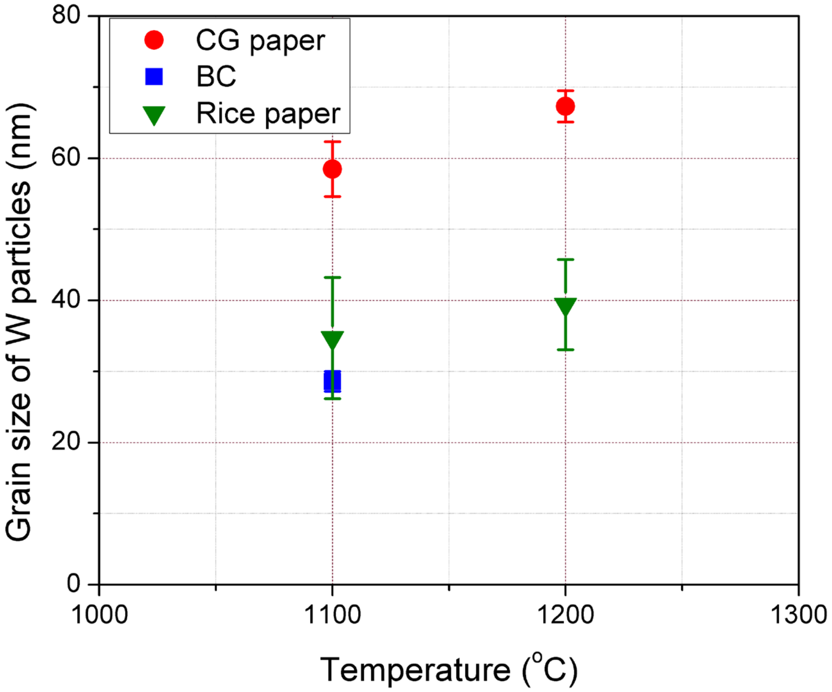

Figure S2: Grain size of the W particles at different temperature for the biopolymers. The grain size was estimated using the Scherrer equation as shown in Equation 2.

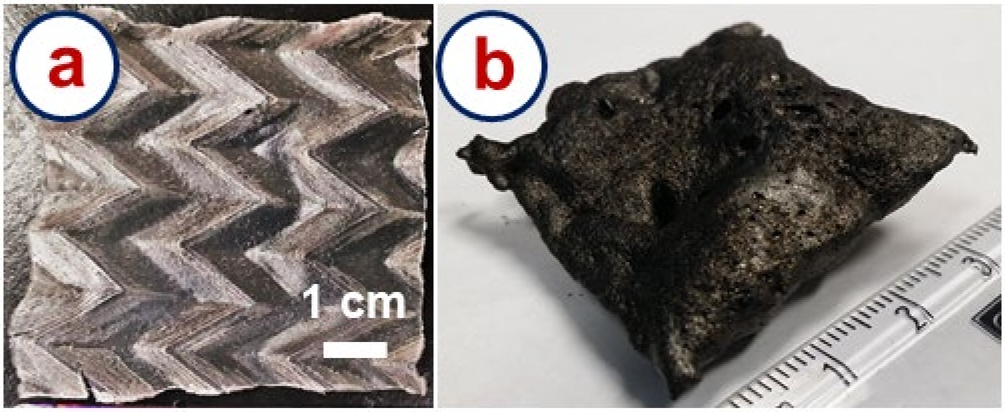

Figure S3: (a) Miura-ori shape fabricated by molding a wet rice paper followed by drying. (b) Carbonized rice paper Miura-ori showing the rice paper loses the shape during the carbonization due to the volumetric expansion of the carbon during carbonization.